A critical technical analysis of two-step thermochemical fuel production cycles
Supplementary Information

A. Lidor[a,*], B. Bulfin[b]
[a] National Renewable Energy Laboratory, 15013 Denver West Parkway, Golden, CO, 80401, USA
[b] School of Chemistry & Environmental Research Institute, University College Cork, Cork, Ireland

Nomenclature

Roman symbols

f	Energy term fraction
h	Specific enthalpy (mass based), $\mathrm{J\,kg^{-1}}$
HHV	Higher heating value, $\mathrm{J\,mol^{-1}}$
m	Mass, kg
n	Amount, mol
$\dot{n}$	Molar flow rate, $\mathrm{mol\,s^{-1}}$
p_0	Ambient pressure, bar
p_{reactor}	Reactor pressure, bar
Q	Heat, J
R	Universal gas constant, $\mathrm{kJ\,mol^{-1}\,K^{-1}}$
T	Temperature, K
t	Time, s

Greek symbols

$\varepsilon_{\mathrm{HR}}$	Heat recovery effectiveness (redox material)
$\varepsilon_{\mathrm{HR,gas}}$	Heat recovery effectiveness (gas)
η	Reactor efficiency
η_{blow}	Blower efficiency
$\eta_{\mathrm{heat\text{-}to\text{-}work}}$	Heat-to-work efficiency
η_{pump}	Vacuum pump efficiency

Subscripts

aux	Auxiliary

*Corresponding author. E-mail:alon.lidor@nrel.gov (A. Lidor).

comb Combined process (heat and fuels)

ins Insulation

ox Oxidizer

pump Pumping

red Reduction

rerad Reradiation

sens Sensible heat

sg Sweep gas

Abbreviations

HTF Heat transfer fluid

1 State of the art—Performance indicators

The data needed to calculate the performance indicators were extracted from the data reported by the authors in each study, or in some cases obtained by directly contacting the authors. Where possible, the performance indicators were reported for the same cycle, so it is an indicator of all round performance for a given system. Table 1 gives details about where the data was sourced in each work.

1.1 Bosch PEM electrolysis system

Data for the Bosch PEM electrolysis systems power density used as an example for conventional energy conversion technologies was obtained from the following source: `https://www.bosch-hydrogen-energy.com/electrolysis/`.

This system can produce 23 $\mathrm{kg\,h^{-1}}$ of hydrogen which gives an output power of 913.6 kW in higher heating value. The dimensions of the electrolysis stack are $0.8 \times 0.97 \times 1.50$ metres, which gives a volume of 1.164 $\mathrm{m^3}$. This gives a power density of 785 $\mathrm{kW\,m^{-3}}$.

Table 1 Source of the data used to calculate performance indicators with the citations in order [1, 2, 3, 4, 5, 6, 7, 8, 9, 10, 11, 12, 13].

Source	Efficiency & Power	Reactor Volume	Feedstock Coversion
Gokon et al. 2008	Table 3 row 1	Dimensions in text	NR
Chueh etal. 2010	Fig. 3B and text	Dimensions in text (ESI)	Fig. 2 A
Diver et al. 2010	From Authors	From Authors	Figure 7 b
Miller et al. 2012	Figures 21 and 27	Calculated for 8 rings using dimensions in Diver et al. (2010)	Figure 21 and Table 5
Villasmil et al. 2014	Reported in the text	NR	NR
Hathaway et al. 2016	Abstract & Text	Calculated from mass and porosity reported in text	CO2 flow (text) and CO production (Fig 3)
Koepf et al. 2016	Table 3	From dimensions given in text	NR
Marxer et al. 2017	Abstract	From dimensions given in text	Fig 4. Cumulative conversion
Haeussler et al. 2020	Tab. 1 and Fig. 11 - Cycle CF-NG #32	From dimensions given in text	Figure 6 b, red peak
Schäppi et al. 2021	Reported in the text	Obtained from authors	Extended Data fig 3
Thanda et al. 2022	Reported in the text	Table 1 & abstract	Figure 10
Zoller et al. 2022	Table 1, Joules	Supporting Info: Figure S9	Table 1
Holmes-Gentle et al. 2023	Figure 6, but inluding W_aux	Obtained from authors	Assuming P_{H2O} saturation pressures in both product streams

* Efficiency omits auxiliary work

Reactor acronyms, DI - directly irradiated redox material, ID - indirectly irradiated, FB - fluidized bed, PF - particle flow, PB - packed bed, M - monolith, RC - rotating cylinder

2 Reactor efficiency

The solar-to-syngas energy efficiency is defined as the ratio between the energy of the produced syngas to the required solar energy and all other auxiliary energy input

$$\eta = \frac{n_{\text{fuel}} \text{HHV}_{\text{fuel}}}{Q_{\text{solar}} + Q_{\text{aux}}}. \tag{1}$$

The solar fuel is denoted here as syngas, but it can also be hydrogen, or carbon monoxide—depending on the reactants. It is customary to convert the required auxiliary work to a heat-equivalent term:

$$Q_{\text{aux}} = \frac{W_{\text{aux}}}{\eta_{\text{heat-to-work}}} \tag{2}$$

with $\eta_{\text{heat-to-work}}$ taken as 0.4 [14]. The different auxiliary terms are the required pumping work and/or inert gas separation. In case of H_2O splitting, the energy for the steam generation should be accounted for as well. The required energy for the inert gas separation is:

$$Q_{\text{inert}} = \frac{E_{\text{inert}}}{\eta_{\text{heat-to-work}}} \int \dot{n}_{\text{inert}} \mathrm{d}t \tag{3}$$

with E_{inert} as the required energy for O_2 separation from the inert gas and $\dot{n}_{\text{inert}}$ is the inert gas molar flow rate.

The pumping energy (in term of equivalent heat) is:

$$Q_{\text{pump}} = Q_{\text{vacuum}} + Q_{\text{HTF}} + Q_{\text{sg}} \tag{4}$$

with Q_{vacuum} being the vacuum pumping energy during reduction, Q_{HTF} being the pumping energy for the HTF flow during heat extraction and heat recuperation, and Q_{sg} the pumping energy for the sweep gas. The first term is only relevant for vacuum operated reactors, while the latter is used for sweep gas operated reactors. The middle term is only relevant when heat recovery is used. The vacuum pump energy (in terms of equivalent heat) is:

$$Q_{\text{vacuum}} = \frac{1}{\eta_{\text{heat-to-work}}} \int \left(\frac{RT_{\text{pump}}}{\eta_{\text{pump}}} \right) \dot{n} \ln \left(\frac{p_0}{p_{\text{reactor}}} \right) dt \tag{5}$$

with R as the universal gas constant, T_{pump} the fluid temperature at the vacuum pump, η_{pump} the vacuum pump efficiency, p_0 the ambient pressure, and p_{reactor} the reactor pressure. The vacuum pump efficiency is calculated from [15] as:

$$\eta_{\text{pump}} = A_0 + A_1 \log \left(\frac{p_{\text{reactor}}}{p_0} \right) + A_2 \log \left(\frac{p_{\text{reactor}}}{p_0} \right)^2 + A_3 \log \left(\frac{p_{\text{reactor}}}{p_0} \right)^3 + A_4 \log \left(\frac{p_{\text{reactor}}}{p_0} \right)^4 \tag{6}$$

with the coefficients given in Table 2. We note that this correlation is an approximation of the maximal combined performance envelope of several industrial pumps that have been investigated, and not a specific existing device efficiency.

Table 2 Coefficients for the pump efficiency correlation

Coefficient	Value
A_0	0.30557
A_1	-0.17808
A_2	-0.15514
A_3	-0.03173
A_4	-0.00203

The inert sweep gas pumping energy is calculated as an isentropic process for an ideal gas:

$$Q_{\text{sg}} = \frac{n_{\text{gas}} R}{1 - \kappa} \left(T_{\text{red}} - T_{\text{pump}} \right) \frac{1}{\eta_{\text{heat-to-work}} \eta_{\text{blow}}} \tag{7}$$

with $\eta_{\text{blower}} = 0.95$, κ as the ratio $\kappa = \dfrac{c_p}{c_v}$, and n_{gas} as the total number of moles of gas flowing through the reactor. Of course, in a real system, the pumping work could be estimated using:

$$Q_{\text{sg}} = \frac{1}{\eta_{\text{blow}} \eta_{\text{heat-to-work}}} \int \frac{\dot{m}_{\text{sg}} \Delta p}{\rho_{\text{sg}}} dt \tag{8}$$

with the pressure gradient Δp determined by the reactor and piping configuration and dimensions, using known correlations such as the Ergun equation and others. The HTF pumping energy during heat recovery is neglected, as in our analysis an overall heat recovery effectiveness value ε_{HR} is used.

The oxidizer also needs to be heated from the ambient temperature to the oxidation temperature. This could be achieved by preheating the oxidizer stream (using heat recovered from the reactor outlet, or by an external heating source) or by injecting it into the reactor at a lower temperature. For H_2O splitting, there is also required energy for the vaporization of water into steam. The terms for the oxidizer heating energy requirements are:

$$Q_{\mathrm{ox}} = (1 - \varepsilon_{\mathrm{HR,gas}})\, m_{\mathrm{ox}} \left(\int h_{\mathrm{ox}}(T)\, dT + h_{\mathrm{fg,ox}} \right) \tag{9}$$

with $\varepsilon_{\mathrm{HR,gas}}$ the gas-has heat recovery effectiveness, m_{ox} the total mass of required oxidizer, h_{ox} the oxidizier enthalpy, and $h_{\mathrm{fg,ox}}$ the enthalpy of vaporization (in the case of H_2O splitting). For the case of a sweep gas operated reactor, the required heating of the sweep gas is calculated in the same manner.

The minimum amount of required sweep gas during reduction and the minimum required oxidizer during oxidation are calculated in the same manner as in Bulfin *et al.* [16]. We assume that the feedstock ratio H_2O:CO_2 is identical to the desired product ratio H_2:CO, even though in practice an excess of steam is needed [10]. In fact, making this assumption results in a slightly better performance than for the actual ratios, since H_2O is a more energy intensive oxidizer, requiring significantly larger sensible heating than CO_2.

Incorporating heat recovery into the analysis is performed using effectiveness value, with $\varepsilon_{\mathrm{HR}}$ used for the sensible redox material and $\varepsilon_{\mathrm{HR,gas}}$ for the gas streams. The sensible energy (eq. (22) in the manuscript) is then:

$$\Delta E_{\mathrm{sens,HR}} = (1 - \varepsilon_{\mathrm{HR}})\, m_{\mathrm{redox}} \int_{T_{\mathrm{start}}}^{T_{\mathrm{end}}} c_{p,\mathrm{redox}} dT \tag{10}$$

and the term $(1 - \varepsilon_{\mathrm{HR,gas}})$ is applied to any gas stream heating requirement.

In addition to assuming heat recovery that utilizes the heat in the next redox cycle, we also define combined efficiency for a process which extracts the high-temperature heat at the end of reduction, but uses this heat in a separate process (i.e., process heat or a power block). The combined efficiency is:

$$\eta_{\mathrm{comb}} = \frac{n_{\mathrm{fuel}} \mathrm{HHV}_{\mathrm{fuel}} + \varepsilon_{\mathrm{HR}} Q_{\mathrm{recovered}} \eta_{\mathrm{hw,comb}}}{Q_{\mathrm{solar}} + Q_{\mathrm{aux}}}. \tag{11}$$

A process efficiency $\eta_{\mathrm{hw,comb}}$ is applied to the recovered heat (with a conservative value of 50%), and we also use the same value of $\varepsilon_{\mathrm{HR}}$ in this method, even though recovering the heat for another process which might not require such high quality heat is significantly easier than heat recovery in the redox cycle.

2.1 Baseline values

The brief justifications for the values in Table 3 in the manuscript are described here in detail:

Reduction temperature: Most experimental work employing ceria performed the reduction at temperatures of 1400-1500°C, citing both material limitations as well as increased reradiation losses as reason for this range. Experimental work of cavity receivers is mostly limited to temperature measurement at the back of the receiver [8, 10, 11], hence the actual mean temperature is higher (as evident by modeling work [17]). Hence, to reflect this temperature gradient and allow for a meaningful comparison with experimental work, we have selected this value.

Oxidation temperature: We have chosen a value for which $\Delta G_{\mathrm{ox}} \leq 0$.

O_2 partial pressure (vacuum): The chosen value is an improvement over the state-of-the-art, but keeping within a reasonable range for vacuum pumps [15].

O_2 mole fraction (sweep gas): This is a typical value for a high purity N5.0 grade industrial nitrogen gas.

Concentration ratio: High-temperature concentrating solar thermal applications will require high concentration ratios. We have chosen a value that has been demonstrated at a small-scale, and assumed it could be scaled-up to a larger industrial scale, although that is still under development. For a more detailed analysis on concentrating systems for high-temperature applications, the reader is referred to the excellent paper by Li et al. [18].

Other losses ratio: This value is the fraction of the other losses (transient heating/cooling of insulation, convective/radiative losses from the reactor outer shell, and active cooling) normalized by the *sensible heating of the oxide* (unlike in other studies, which define the loss factor differently such as in [19]). The main reasoning for this definition, is due to different scaling laws of the various energy terms. For example, reradiation losses would scale with aperture size, which is not necessarily identical to the volumetric scaling. Hence, this is not a factor which is limited to values between 0 and 1. The largest and most successful demonstration to date was by Zoller et al. [12]. Using the data from [20] (Fig. 4.14), the value of f_{other} is calculated (summing the 'Other heat losses', 'Conduction to water-cooled front', and 'Sensible heat of reactor components' over 'Sensible heat of RPC') with a value of 0.42. The smaller lab-scale reactor [8] a value of 1.72 is calculated (Fig. 4.10 in [21]). For comparison with values from another work, we converted the loss factor $f = 0.2$ of Li *et al.* [19] to our f_{other} (Fig. 6 in their paper) for our reduction temperature, obtaining a value of 0.44 (higher than our chosen $f_{\text{other}} = 0.3$).

Heat recovery effectiveness (redox material): The justification based on a thermodynamic analysis is detailed in subsection 3.2 of the manuscript.

Heat recovery effectiveness (gas-to-gas): High-temperature gas-to-gas heat recovery of gases with low specific heat capacity and relatively low flow rates will be limited in their heat exchanger effectiveness, unless extremely large surface areas will be used [22, 23]. Hence, we follow the accepted values in the literature [24, 16, 19].

Oxidation extent:

Heat-to-work efficiency: This value is based on the accepted value in the literature [14].

2.2 Additional figures for energy balance and efficiency maps

In this subsection additional figures for the energy balance and efficiency maps are presented:

- Figure 1 presents the energy breakdown for sweep gas operated reactor as a function of f_{other} and $\varepsilon_{\text{heat-recovery}}$.
- Figure 2 presents the energy breakdown for sweep gas operated reactor as a function of T_{ox} and C.
- Figure 3 presents the efficiency maps for vacuum and sweep gas operated reactors as a function of p_{O_2} and C.
- Figure 4 presents the efficiency maps for vacuum and sweep gas operated reactors as a function of p_{O_2} and f_{other}.

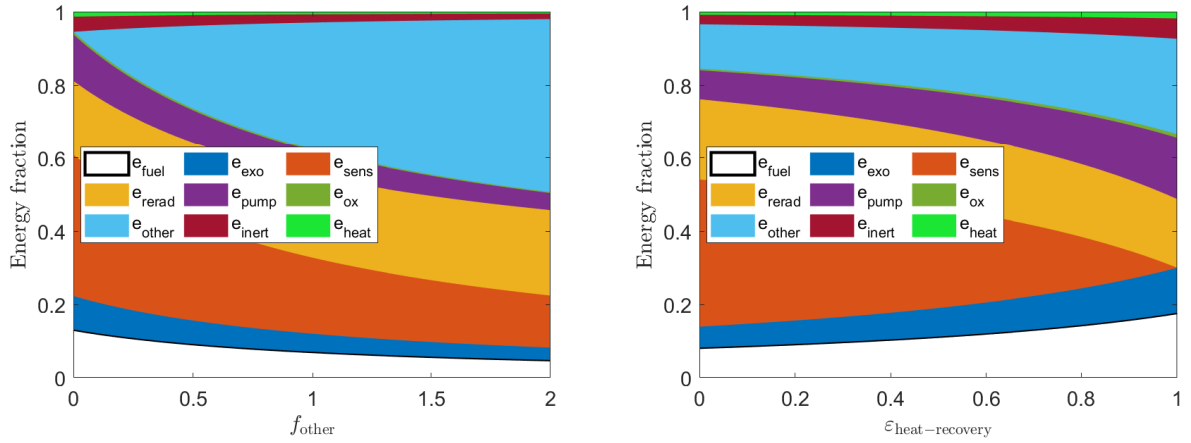

(a) (b)

Figure 1 Reactor efficiency η and energy breakdown for a sweep gas operated reactor as a function of (a) f_{other}, and (b) ε_{HR}. The analysis performed for the baseline cycle (Table 3 in the manuscript).

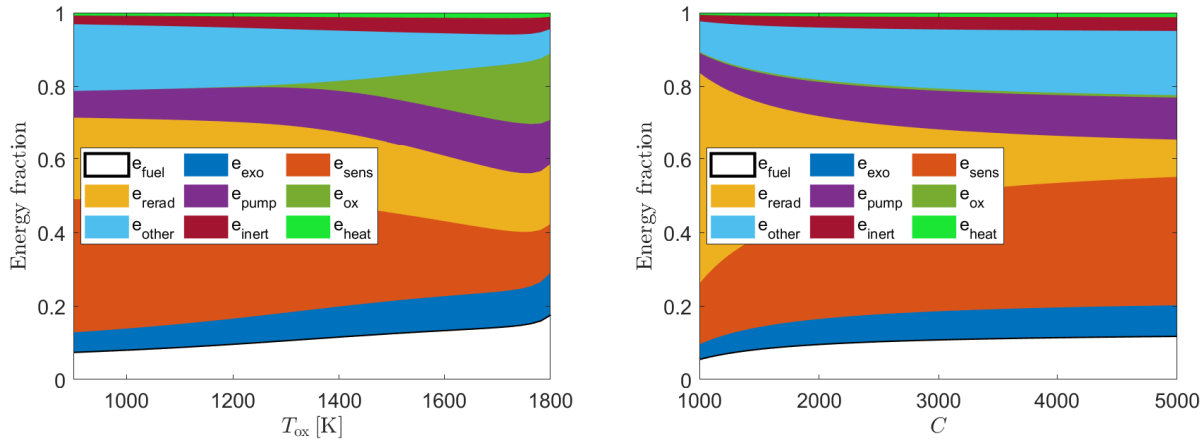

(a) (b)

Figure 2 Reactor efficiency η and energy breakdown for a sweep gas operated reactor as a function of (a) T_{ox}, and (b) C. The analysis performed for the baseline cycle (Table 3 in the manuscript).

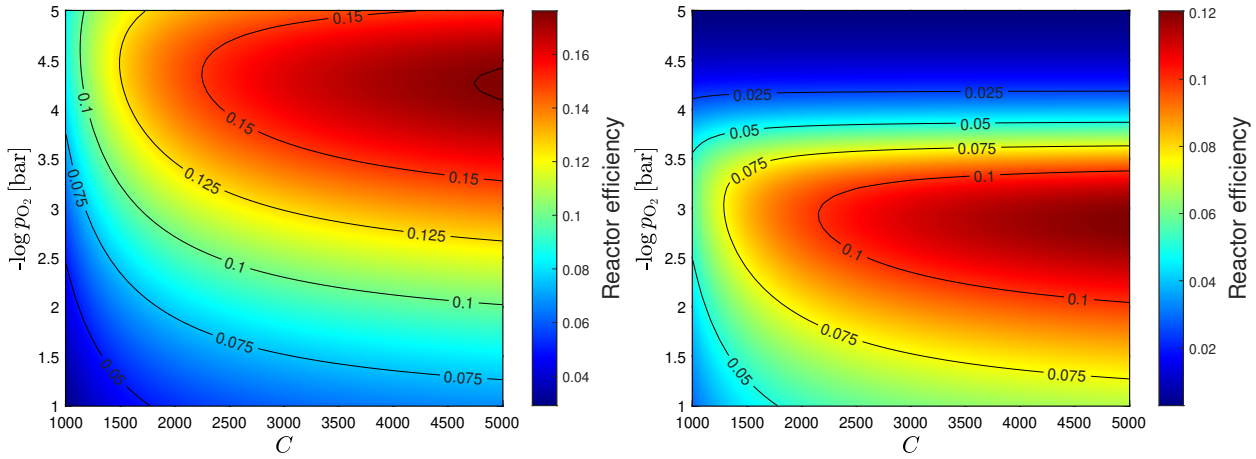

(a) (b)

Figure 3 Reactor efficiency η as a function of C and p_{O_2} for (a) a vacuum operated reactor and (b) sweep gas operated reactor. The analysis is performed for the baseline cycle (Table 3 in the manuscript).

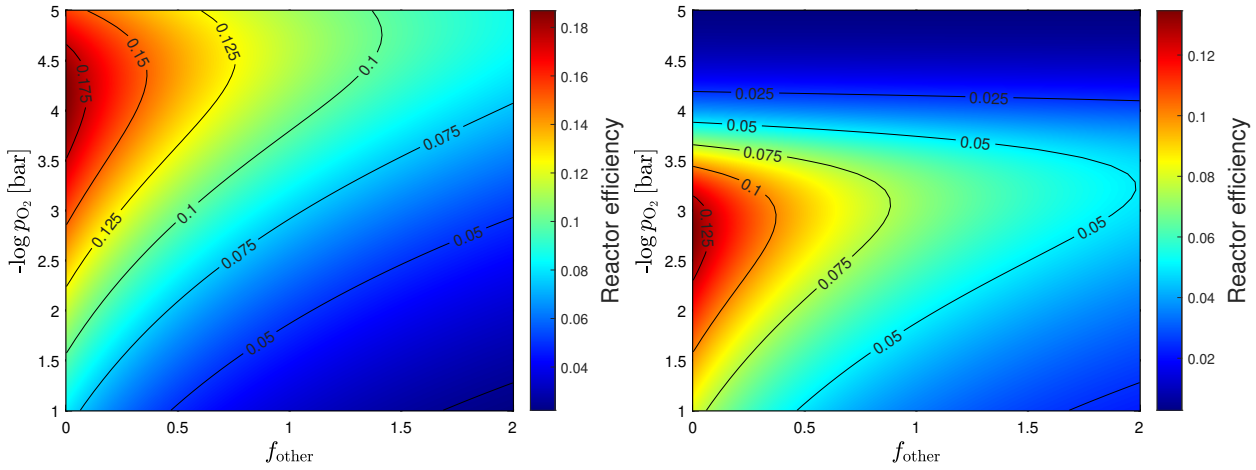

(a) (b)

Figure 4 Reactor efficiency η as a function of f_{other} and p_{O_2} for (a) a vacuum operated reactor and (b) sweep gas operated reactor. The analysis is performed for the baseline cycle (Table 3 in the manuscript).

3 Effect of heat recovery on reactor efficiency

3.1 Heat recovery assuming only redox material sensible heat

We use our defined ratio of the redox material sensible heating required to the solar energy input as:

$$f_{\text{sens}} = \frac{\Delta E_{\text{sens}}}{Q_{\text{solar}}}. \tag{12}$$

We can calculate the reactor energy efficiency with heat recovery per:

$$\eta_{\text{with-HR}} = \frac{n_{\text{fuel}}\text{HHV}_{\text{fuel}}}{(1-\varepsilon_{\text{HR}})\,\Delta E_{\text{sens}} + \Delta E_{\text{red}} + \Delta E_{\text{ins}} + Q_{\text{loss}} + Q_{\text{rerad}} + W_{\text{aux}}}. \tag{13}$$

If we divide the reactor efficiency with heat recovery by the reactor efficiency without any heat recovery, we get:

$$\frac{\eta_{\text{with-HR}}}{\eta} = \frac{\Delta E_{\text{sens}} + \Delta E_{\text{red}} + \Delta E_{\text{ins}} + Q_{\text{loss}} + Q_{\text{rerad}} + W_{\text{aux}}}{(1-\varepsilon_{\text{HR}})\,\Delta E_{\text{sens}} + \Delta E_{\text{red}} + \Delta E_{\text{ins}} + Q_{\text{loss}} + Q_{\text{rerad}} + W_{\text{aux}}}. \tag{14}$$

We know that $Q_{\text{solar}} \gg W_{\text{aux}}$. We can then neglect W_{aux} compared to the sum of the other terms (which are the individual contributions for Q_{solar}) and write:

$$\frac{\eta_{\text{with-HR}}}{\eta} = \frac{\Delta E_{\text{sens}} + \Delta E_{\text{red}} + \Delta E_{\text{ins}} + Q_{\text{loss}} + Q_{\text{rerad}}}{(1-\varepsilon_{\text{HR}})\,\Delta E_{\text{sens}} + \Delta E_{\text{red}} + \Delta E_{\text{ins}} + Q_{\text{loss}} + Q_{\text{rerad}}}. \tag{15}$$

Now we can use the term from eq. 12 to write:

$$\frac{\eta_{\text{with-HR}}}{\eta} = \frac{1}{1 - f_{\text{sens}}\varepsilon_{\text{HR}}}. \tag{16}$$

3.2 Heat recovery assuming redox material and insulation heat

The ratio of the redox material and insulation sensible heating required over the solar energy input is:

$$f_{\text{sens}} = \frac{\Delta E_{\text{sens}} + \Delta E_{\text{ins}}}{Q_{\text{solar}}}. \tag{17}$$

The rest of the following mathematical development is identical to the one for the previous case. We can calculate the reactor efficiency with heat recovery per:

$$\eta_{\text{with-HR}} = \frac{n_{\text{fuel}}\text{HHV}_{\text{fuel}}}{(1-\varepsilon_{\text{HR}})\,(\Delta E_{\text{sens}} + \Delta E_{\text{ins}}) + \Delta E_{\text{red}} + Q_{\text{loss}} + Q_{\text{rerad}} + W_{\text{aux}}} \tag{18}$$

with ε_{HR} as the heat recovery effectiveness, i.e. how much of the redox material sensible heat is recovered and utilized in the next cycle. It is possible to divide this term by the standard definition for η to get:

$$\frac{\eta_{\text{with-HR}}}{\eta} = \frac{\Delta E_{\text{sens}} + \Delta E_{\text{red}} + \Delta E_{\text{ins}} + Q_{\text{loss}} + Q_{\text{rerad}} + W_{\text{aux}}}{(1-\varepsilon_{\text{HR}})\,(\Delta E_{\text{sens}} + \Delta E_{\text{ins}}) + \Delta E_{\text{red}} + Q_{\text{loss}} + Q_{\text{rerad}} + W_{\text{aux}}}. \tag{19}$$

If we neglect W_{aux} compared to the other terms (which are the individual contributions for Q_{solar}), we can write:

$$\frac{\eta_{\text{with-HR}}}{\eta} = \frac{\Delta E_{\text{sens}} + \Delta E_{\text{red}} + \Delta E_{\text{ins}} + Q_{\text{loss}} + Q_{\text{rerad}}}{(1-\varepsilon_{\text{HR}})\left(\Delta E_{\text{sens}} + \Delta E_{\text{ins}}\right) + \Delta E_{\text{red}} + Q_{\text{loss}} + Q_{\text{rerad}}}. \tag{20}$$

Now we can use the term from eq. 17 to write:

$$\frac{\eta_{\text{with-HR}}}{\eta} = \frac{1}{1 - f_{\text{sens}}\varepsilon_{\text{HR}}}. \tag{21}$$

Rearranging the equation we can see the effect of heat recovery on η by:

$$\eta_{\text{with-HR}} = \frac{\eta}{1 - f_{\text{sens}}\varepsilon_{\text{HR}}}. \tag{22}$$

As seen in the previous section, we can see that increasing the value of ε_{HR} is beneficial for increasing the η. This case can be considered the most ideal case since we assume that the heat recovery is effective both for the redox material sensible heat and the insulation heat in the same manner. The realistic value probably lies somewhere between these two extremes. Since the sensible heat of the insulation is probably not recovered with the same effectiveness as the redox material sensible heat, and also should be minimized in an ideal reactor, the approach shown before could be extended to a case with two different parameters, f_{sens} (as in eq. 12) and $f_{\text{ins}} = \Delta E_{\text{ins}}/Q_{\text{solar}}$, and two different heat recovery effectiveness values $\varepsilon_{\text{HR,sens}}$ and $\varepsilon_{\text{HR,ins}}$, to yield the following:

$$\frac{\eta_{\text{with-HR}}}{\eta} = \frac{1}{1 - f_{\text{sens}}\varepsilon_{\text{HR,sens}} - f_{\text{ins}}\varepsilon_{\text{HR,ins}}}. \tag{23}$$

The values of f_{sens} and f_{ins} for the examples used in comparison are taken from [21, 8, 25, 12].

3.3 Thermodynamic limits on heat recovery

We consider here the case in which heat is extracted from a solar reactor at the end of reduction, stored, and reused after oxidation. We focus on the demonstration of a specific heat recovery method of using an inert HTF with a stationary volumetric solar reactor, such as in Lidor *et al.* [26, 27]. The control volume (CV) and a schematic plot of the temperatures during the process are presented in Figure 5. We assume the following: (a) no heat losses from the system to the ambient; (b) the entropy of the gas remaining inside the CV at the end is negligible compared to the entropy of the redox material; (c) only the redox material participates in the heat extraction (i.e., not heat is transferred from the insulation); (d) the specific heat capacity of both redox material and HTF is constant; (e) the HTF is an ideal gas; and (f) the redox material temperature is uniform. Assuming a CV over the solar reactor and TES unit during heat extraction we can write the rate of entropy generation due to irreversiblities (following [28])

$$\dot{S}_{\text{gen}} = \frac{dS}{dt} - \sum_{i=0}^{n} \frac{\dot{Q}_i}{T_i} - \sum_{\text{in}} \dot{m}s + \sum_{\text{out}} \dot{m}s \geq 0. \tag{24}$$

Following our assumptions, this term we receive is:

$$\dot{S}_{\text{gen}} = \frac{m_{\text{redox}} C_{p,\text{redox}}}{T_{\text{redox}}} \frac{dT_{\text{redox}}}{dt} - \dot{m}\left(s_{\text{in}} - s_{\text{out}}\right). \tag{25}$$

By using the relations for an ideal gas we can write:

$$\dot{S}_{\text{gen}} = \frac{m_{\text{redox}} C_{p,\text{redox}}}{T_{\text{redox}}} \frac{dT_{\text{redox}}}{dt} + \dot{m}c_p \ln \frac{T_{\text{out}}}{T_{\text{in}}}. \tag{26}$$

We follow Bejan's formulation for the entropy generation number:

$$N_S = \frac{\text{exergy/availability destroyed}}{\text{total availability from the process}} \tag{27}$$

which in our case can be written as:

$$N_S = \frac{T_0 \int_0^t \dot{S}_{\text{gen}} dt}{Q_{\text{sens}}}. \tag{28}$$

By choosing Q_{sens} as the total availability from the process we assume the most ideal case, so in practice this allows us to set an upper bound efficiency for the heat extraction process. We define the outlet temperature T_{out} using a time-dependent linear correlation based on [26] and use the values from their experiment ($\dot{m}_{\text{HTF}} = 7.5$ kg h^{-1}, $T_{\text{red}} = 1550$ K, $T_{\text{ox}} = 1223$ K, and $t_{\text{extraction}} = 360$ s). As an ideal case, we take the total availability is the heat from the redox material, as this would also be heat needed to recuperate back into the reactor. Solving the above integral yields a values of $N_S = 0.4286$, and by using the relation $\eta_{\text{II,HE}} = 1 - N_S$ we receive a second law efficiency $\eta_{\text{II}} = 0.5714$. Since it was observed in the experiment that the HTF was slightly heated in the nozzle entering the reactor, we calculate the efficiency with $T_{\text{in}} = 450$ K, yielding $N_S = 0.2712$ and $\eta_{\text{II,HE}} = 0.7288$.

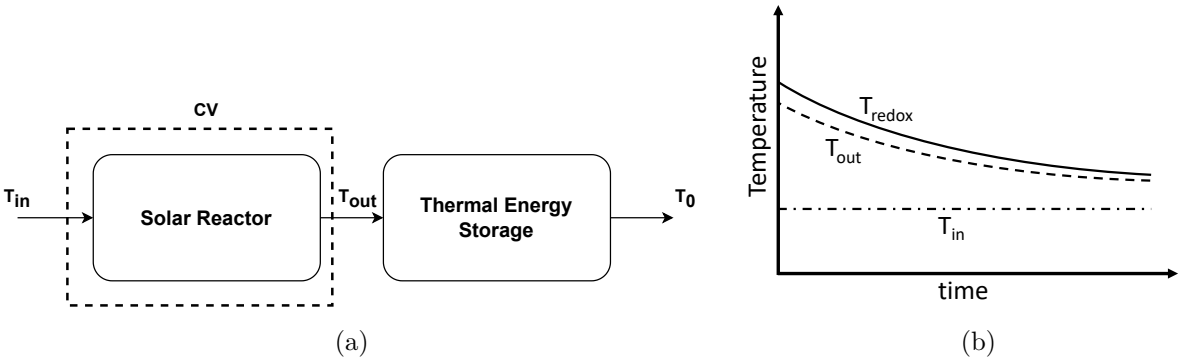

(a) (b)

Figure 5 Thermodynamics of heat extraction from a solar reactor: (a) the CV over the system, and (b) the schematic temperature evolution over time.

To generalize this calculation and study the effects of various parameters such as HTF flow rate and duration, one would need to develop the actual terms for T_{redox} and T_{out}, based on the heat transfer mechanisms within the reactor. If we assume that the heat extraction can be done in an identical manner but at a shorter duration, the second law efficiency would increase. However, in a real system, changing such a parameter would affect multiple other values.

It is important to note that in addition to our extremely lenient assumptions (e.g., no heat losses during the process), we have made some inherent ideal (and unrealistic) assumptions in order to close the cycle, i.e. no exergy destroyed during the TES charge/discharge cycle and no exergy destroyed during the recuperation back into the reactor.

This interesting thermodynamic problem merits further study, as a more detailed analysis of the complete cycle, over both reactor and TES, could provide the theoretical upper boundary of such sensible heat storage systems. One must remember that in the applications for high-temperature solar thermochemistry, it is not the amount of heat that is recovered so much as its quality that matters. Recovering even 90% of the heat, but at temperatures below the oxidation temperature, would be useless in lowering the amount of sensible heating that the redox material would need and improving the reactor efficiency.

4 Power density and system scale-up

The production of synthetic fuels via the Fischer-Tropsch (FT) synthesis is a complex process, yielding different types of synthetic crude based on syngas composition, process temperature, reactor design,

and choice of catalyst, to name a few [29, 30]. In addition, it requires multiple consecutive steps, similar to that of an oil refinery, to reach the final products. It is near impossible to receive only a single fuel product via FT, however we take an ideal case assuming full conversion of syngas to jet fuel $X_{\text{syngas-to-fuel}} = 1$. In addition, we base our process energy efficiency, on a simple chemical reactor efficiency calculation. The numerous required operating steps from the FT synthesis unit until a final product [29, 30] are not included in our analysis, and in practice would further increase the energy input requirements. We use the simplified model reaction for Fischer-Tropsch (FT) synthesis to calculate the mass balance over the fuel synthesis unit [31]:

$$\mathrm{CO} + \left(1 + \frac{m}{2n}\right) \mathrm{H_2} \rightarrow \frac{1}{n} \mathrm{C}_n \, \mathrm{H}_m + \mathrm{H_2O} \tag{29}$$

with a model composition of $\mathrm{C_{11}H_{22}}$ [32] and $\Delta_\mathrm{r} H = -165\ \mathrm{kJ\,mol^{-1}}$. This gives us the following fuel yield:

$$n_{\text{fuel}} = \frac{1}{11} X_{\text{syngas-to-fuel}} n_{\mathrm{CO}} \tag{30}$$

with n_{syngas} as the amount of syngas entering the FT reactor and $X_{\text{syngas-to-fuel}}$ as the FT conversion extent. The energy of the produced fuel is thus:

$$Q_{\text{fuel}} = n_{\text{fuel}} \mathrm{LHV}_{\text{fuel}} = \frac{X_{\text{syngas-to-fuel}} n_{\mathrm{CO}} \mathrm{LHV}_{\text{fuel}}}{11} \tag{31}$$

with $\mathrm{LHV}_{\text{fuel}}$ as the molar-based heating value of the fuel. We can also write it in terms of the reduction extent and required amount of redox material:

$$Q_{\text{fuel}} = \frac{X_{\text{syngas-to-fuel}} n_{\text{redox}} \alpha \Delta\delta \mathrm{LHV}_{\text{fuel}}}{11} \frac{\nu_{\mathrm{CO}}}{\nu_{\mathrm{CO}} + \nu_{\mathrm{H_2}}} \tag{32}$$

with n_{redox} the amount of redox material, α the extent of re-oxidation ($\alpha = 1$ for full re-oxidation), $\Delta\delta = \delta_{\text{red}} - \delta_{\text{ox}}$, ν_{CO} as the CO stoichiometric coefficient, and $\nu_{\mathrm{H_2}}$ as the $\mathrm{H_2}$ stoichiometric coefficient. The use of the stoichiometric coefficients is required here since 1 mol of syngas only has 1/3 mol of CO. The amount of produced fuel is then:

$$n_{\text{fuel}} = \frac{X_{\text{syngas-to-fuel}} n_{\text{redox}} \alpha \Delta\delta}{11} \frac{\nu_{\mathrm{CO}}}{\nu_{\mathrm{CO}} + \nu_{\mathrm{H_2}}}. \tag{33}$$

We can rearrange it to calculate the required amount of redox material we need to process a given amount of fuel:

$$\frac{n_{\text{redox}}}{n_{\text{fuel}}} = \frac{11}{X_{\text{syngas-to-fuel}} \alpha \Delta\delta} \frac{\nu_{\mathrm{CO}} + \nu_{\mathrm{H_2}}}{\nu_{\mathrm{CO}}}. \tag{34}$$

We note that it is not clear whether previous studies examining the scale-up potential performed the mass balance analysis on the FT unit, or just followed an overall energy balance on the complete system (using a system efficiency that includes the energy conversion efficiencies of each step). At least in some cases, it is apparent from the text that the energy balance approach was used. It is important to remember that in a chemical conversion process such as FT synthesis, the amount of product is much smaller than the amount of reactants due to the molecules composition (low number of C and H in the syngas stream, and high number of C and H in the product stream). This is highlighted by the example of the American Hydrocol facility which converted $75\,500\,\mathrm{m^3\,h^{-1}}$ of natural gas into $38\,\mathrm{m^3\,h^{-1}}$ of motor gasoline, $8\,\mathrm{m^3\,h^{-1}}$ diesel, and $2.8\,\mathrm{t\,h^{-1}}$ of oxygenates (approximately $3.5\,\mathrm{m^3\,h^{-1}}$), and was considered successful and efficient [30].

We continue to examine the specific redox mass, energy and power properties, as they predict the required sizing of the solar fuel plant and amount of redox material needed to produce a given amount of fuel. In our analysis, we focus on the following metrics: (a) required mass of redox material per fuel volume; (b) required mass of redox material per reactor power output; (c) required solar energy per fuel volume; and (d) required solar power per fuel volume.

Required redox material per fuel volume: The amount of redox material that needs to undergo one complete cycle per volume of fuel produced is an illustrative parameter, since it can shed important light on the scale-up potential of the technology. This can be calculated in the form of required mass per volume:

$$\frac{m_{\text{redox}}}{V_{\text{fuel}}} = 11\frac{M_{\text{redox}}}{M_{\text{fuel}}}\frac{\rho_{\text{fuel}}}{X_{\text{syngas-to-fuel}}\alpha\Delta\delta}\frac{\nu_{\text{CO}}+\nu_{\text{H}_2}}{\nu_{\text{CO}}}. \tag{35}$$

For each liter of produced jet fuel, 919 kg of ceria must undergo redox. For example, a typical long-haul 10 hours flight of a Boeing 747 requires approximately 150 000 L of Jet A-1 aviation fuel. Assuming CeO_2 as the redox material with the input per baseline case in the manuscript, we find out that 138 kt of CeO_2 are needed to undergo one redox cycle to produce this amount of aviation fuel. Of high interest is the fact that the reactor efficiency does not play a role here, as this value is determined from cycle time and oxygen stored which is determined by the thermodynamic limitations of the redox process. Of course, this amount can be divided into multiple reactors and cycles, but it still provides insight into the required scale.

Required solar energy input per fuel volume: The required solar energy to generate one liter of fuel by can be calculated using the overall system efficiency η_{system}, including optical, reactor, and fuel synthesis efficiencies,

$$\frac{Q_{\text{solar}}}{V_{\text{fuel}}} = \frac{\text{LHV}_{\text{fuel}}\rho_{\text{fuel}}}{\eta_{\text{opt}}\eta_{\text{reactor}}\eta_{\text{syngas-to-fuel}}}. \tag{36}$$

While in practice Q_{solar} here includes also the auxiliary energy, we have seen that in most cases it is negligible compared to the solar energy input. Additionally, this energy must be supplied, and following the convention in the field of solar fuels, the auxiliary work is assumed to be driven by heat, using $\eta_{\text{heat-to-work}}$. For producing Jet A-1 fuel with the standard we get a value of 694 MJ L^{-1}, meaning we need to invest 694 MJ of solar energy to produce a single liter of aviation jet fuel (and that is excluding the energy for CO_2 and water capture, pumping, gas separation, and compression). This indicator can be used to estimate how much fuel can be produced based on solar energy availability.

Annual production of jet fuel: For the annual production performance metrics we use the relations developed for the specific parameters, and multiply them by the design producton capacity, as well as normalizing per annual operation time ($t_{\text{plant}} = t_{\text{year}} f_{\text{capacity}}$). The total required redox material mass to meet this annual production is given by,

$$m_{\text{redox-required}} = \frac{m_{\text{redox}}}{V_{\text{fuel}}}\frac{V_{\text{fuel,annual}} t_{\text{cycle}}}{t_{\text{plant}}}, \tag{37}$$

the required annual solar energy is:

$$Q_{\text{solar,annual}} = \frac{Q_{\text{solar}}}{V_{\text{fuel}}} V_{\text{fuel}}, \tag{38}$$

with the required solar energy per cycle as:

$$Q_{\text{solar,cycle}} = Q_{\text{solar,annual}}\frac{t_{\text{cycle}}}{t_{\text{plant}}}. \tag{39}$$

By knowing how much energy per cycle we need and the cycle duration, we can estimate the required solar power input:

$$P_{\text{solar,required}} = \frac{Q_{\text{solar,cycle}}}{t_{\text{cycle}}}. \tag{40}$$

For supporting the assumption that a continuous usage of the solar radiative power input is utilized, we calculate the number of rectors that must operate in parallel during a single cycle as:

$$n_{\text{reactors}} = \frac{t_{\text{cycle}}}{t_{\text{red}}}. \tag{41}$$

References

[1] N. Gokon, S. Takahashi, H. Yamamoto, T. Kodama, Thermochemical two-step water-splitting reactor with internally circulating fluidized bed for thermal reduction of ferrite particles, International Journal of Hydrogen Energy 33 (9) (2008) 2189–2199.

[2] W. C. Chueh, C. Falter, M. Abbott, D. Scipio, P. Furler, S. M. Haile, A. Steinfeld, High-flux solar-driven thermochemical dissociation of CO_2 and H_2O using ceria redox reactions, Science 330 (6012) (2010) 1797–1801. doi:10.1123/science.1197834.

[3] R. B. Diver, J. E. Miller, N. P. Siegel, T. A. Moss, Testing of a CR5 Solar Thermochemical Heat Engine Prototype, in: ASME 2010 4th International Conference on Energy Sustainability, Volume 2, ASMEDC, 2010, pp. 97–104. doi:10.1115/ES2010-90093.

[4] J. Miller, M. Allendorf, A. Ambrosini, E. Coker, R. Diver, Jr, I. Ermanoski, L. Evans, R. Hogan, Jr, A. McDaniel, Development and assessment of solar-thermal-activated fuel production. Phase 1, summary., Tech. Rep. SAND2012-5658, 1055617, Sandia National Laboratories (SNL), Albuquerque, NM, and Livermore, CA (United States) (Jul. 2012). doi:10.2172/1055617.

[5] W. Villasmil, A. Meier, A. Steinfeld, Dynamic modeling of a solar reactor for zinc oxide thermal dissociation and experimental validation using IR thermography, Journal of solar energy engineering 136 (1) (2014) 010901.

[6] B. J. Hathaway, R. Bala Chandran, A. C. Gladen, T. R. Chase, J. H. Davidson, Demonstration of a Solar Reactor for Carbon Dioxide Splitting via the Isothermal Ceria Redox Cycle and Practical Implications, Energy & Fuels 30 (8) (2016) 6654–6661. doi:10.1021/acs.energyfuels.6b01265.

[7] E. Koepf, W. Villasmil, A. Meier, Pilot-scale solar reactor operation and characterization for fuel production via the Zn/ZnO thermochemical cycle, Applied Energy 165 (2016) 1004–1023. doi:10.1016/j.apenergy.2015.12.106.

[8] D. Marxer, P. Furler, M. Takacs, A. Steinfeld, Solar thermochemical splitting of CO_2 into separate streams of CO and O_2 with high selectivity, stability, conversion, and efficiency, Energy Environ. Sci. 10 (5) (2017) 1142–1149. doi:10.1039/C6EE03776C.

[9] A. Haeussler, S. Abanades, A. Julbe, J. Jouannaux, B. Cartoixa, Solar thermochemical fuel production from H2O and CO2 splitting via two-step redox cycling of reticulated porous ceria structures integrated in a monolithic cavity-type reactor, Energy 201 (2020) 117649.

[10] R. Schäppi, D. Rutz, F. Dähler, A. Muroyama, P. Haueter, J. Lilliestam, A. Patt, P. Furler, A. Steinfeld, Drop-in Fuels from Sunlight and Air, Nature 601 (7891) (2021) 1–6. doi:10.1038/s41586-021-04174-y.

[11] V. Thanda, T. Fend, D. Laaber, A. Lidor, H. von Storch, J. Säck, J. Hertel, J. Lampe, S. Menz, G. Piesche, S. Berger, S. Lorentzou, M. Syrigou, T. Denk, A. Gonzales-Pardo, A. Vidal, M. Roeb, C. Sattler, Experimental investigation of the applicability of a 250 kW ceria receiver/reactor for solar thermochemical hydrogen generation, Renewable Energy 198 (August) (2022) 389–398. doi:10.1016/j.renene.2022.08.010.

[12] S. Zoller, E. Koepf, D. Nizamian, M. Stephan, A. Patané, P. Haueter, M. Romero, J. Gonzalez-Aguilar, D. Lieftink, E. de Wit, S. Brendelberger, A. Sizmann, A. Steinfeld, A solar tower fuel plant for the thermochemical production of kerosene from H_2O and CO_2, Joule 6 (2022) 1–11. doi:10.1016/j.joule.2022.06.012.

[13] I. Holmes-Gentle, S. Tembhurne, C. Suter, S. Haussener, Kilowatt-scale solar hydrogen production system using a concentrated integrated photoelectrochemical device, Nature Energy (2023) 1–11.

[14] B. Bulfin, M. Miranda, A. Steinfeld, Performance Indicators for Benchmarking Solar Thermochemical Fuel Processes and Reactors, Frontiers in Energy Research 9 (July) (2021) 1–12. doi:10.3389/fenrg.2021.677980.

[15] S. Brendelberger, H. von Storch, B. Bulfin, C. Sattler, Vacuum pumping options for application in solar thermochemical redox cycles – Assessment of mechanical-, jet- and thermochemical pumping systems, Solar Energy 141 (2017) 91–102. doi:10.1016/j.solener.2016.11.023.

[16] B. Bulfin, F. Call, M. Lange, O. Lübben, C. Sattler, R. Pitz-Paal, I. V. Shvets, Thermodynamics of CeO_2 Thermochemical Fuel Production, Energy & Fuels 29 (2) (2015) 1001–1009. doi:10.1021/ef5019912.

[17] S. Zoller, E. Koepf, P. Roos, A. Steinfeld, Heat Transfer Model of a 50 kW Solar Receiver–Reactor for Thermochemical Redox Cycling Using Cerium Dioxide, Journal of Solar Energy Engineering 141 (2) (2019) 021014. doi:10.1115/1.4042059.

[18] L. Li, B. Wang, J. Pye, W. Lipiński, Temperature-based optical design, optimization and economics of solar polar-field central receiver systems with an optional compound parabolic concentrator, Solar energy 206 (2020) 1018–1032.

[19] S. Li, V. M. Wheeler, P. B. Kreider, R. Bader, W. Lipiński, Thermodynamic Analyses of Fuel Production via Solar-Driven Non-stoichiometric Metal Oxide Redox Cycling. Part 2. Impact of Solid–Gas Flow Configurations and Active Material Composition on System-Level Efficiency, Energy & Fuels 32 (10) (2018) 10848–10863. doi:10.1021/acs.energyfuels.8b02082.

[20] S. Zoller, A 50 kW Solar Thermochemical reactor for Syngas Production utilizing Porous Ceria Structures, Phd thesis, ETH Zürich (2019).

[21] D. A. Marxer, 4 kW solar reactor technology for splitting of H_2O and CO_2 with a temperature – pressure swing redox cycle, Ph.D. thesis, ETH Zürich (2016). doi:10.3929/ETHZ-A-010867020.

[22] T. L. Bergman, F. P. Incropera, D. P. DeWitt, A. S. Lavine, Fundamentals of Heat and Mass Transfer, John Wiley & Sons, 2011.

[23] W. M. Rohsenow, J. P. Hartnett, Y. I. Cho (Eds.), Handbook of Heat Transfer, 3rd Edition, McGraw-Hill Handbooks, McGraw-Hill, New York, 1998.

[24] I. Ermanoski, J. Miller, M. Allendorf, Efficiency maximization in solar-thermochemical fuel production: challenging the concept of isothermal water splitting, Physical Chemistry Chemical Physics 16 (18) (2014) 8418–8427.

[25] S. Zoller, A 50 kW Solar Thermochemical Reactor for Syngas Production Utilizing Porous Ceria Structures, Doctoral Thesis, ETH Zurich, accepted: 2020-07-16T08:20:41Z (2020). doi:10.3929/ethz-b-000426499.

[26] A. Lidor, Y. Aschwanden, J. Häseli, P. Reckinger, P. Haueter, A. Steinfeld, High-temperature heat recovery from a solar reactor for the thermochemical redox splitting of H_2O and CO_2, Applied Energy 329 (November 2022) (2023) 120211. doi:10.1016/j.apenergy.2022.120211.

[27] A. Lidor, L. Zimmermann, Experimental demonstration of high-temperature heat recovery in a solar reactor, Solar Energy 262 (2023) 111915. doi:10.1016/j.solener.2023.111915.

[28] A. Bejan, Advanced Engineering Thermodynamics, 1st Edition, Wiley, 2016. doi:10.1002/9781119245964.

[29] A. Steynberg, M. Dry, Fischer-Tropsch Technology, Elsevier, 2004.
URL https://www.sciencedirect.com/bookseries/studies-in-surface-science-and-catalysis/vol/152/suppl/C

[30] A. de Klerk, Fischer-Tropsch Refining, Wiley, 2011. doi:10.1002/9783527635603.
URL https://onlinelibrary.wiley.com/doi/book/10.1002/9783527635603

[31] M. A. Fahim, T. A. Alsahhaf, A. Elkilani, Fundamentals of Petroleum Refining, Elsevier, 2010. doi:10.1016/C2009-0-16348-1.
URL https://linkinghub.elsevier.com/retrieve/pii/C20090163481

[32] R. Xu, K. Wang, S. Banerjee, J. Shao, T. Parise, Y. Zhu, S. Wang, A. Movaghar, D. J. Lee, R. Zhao, X. Han, Y. Gao, T. Lu, K. Brezinsky, F. N. Egolfopoulos, D. F. Davidson, R. K. Hanson, C. T. Bowman, H. Wang, A physics-based approach to modeling real-fuel combustion chemistry – II. Reaction kinetic models of jet and rocket fuels, Combustion and Flame 193 (2018) 520–537. doi:10.1016/j.combustflame.2018.03.021.